TECHNICAL REPORT ARLCB-TR-82023

EFFECTS OF R-RATIO ON CRACK INITIATION AT EXTERNAL DISCONTINUITIES IN AUTOFRETTAGED CYLINDERS

Robert R. Fujczak

July 1982

US ARMY ARMAMENT RESEARCH AND DEVELOPMENT COMMAND
LARGE CALIBER WEAPON SYSTEMS LABORATORY
BENÉT WEAPONS LABORATORY
WATERVLIET, N. Y. 12189

DISCLAIMER

The findings in this report are not to be construed as an official Department of the Army position unless so designated by other authorized documents.

The use of trade name(s) and/or manufacture(s) does not constitute an official indorsement or approval.

DISPOSITION

Destroy this report when it is no longer needed. Do not return it to the originator.

REPORT DOCUMENTATION PAGE		READ INSTRUCTIONS BEFORE COMPLETING FORM
1. REPORT NUMBER ARLCB-TR-82023	2. GOVT ACCESSION NO.	3. RECIPIENT'S CATALOG NUMBER
4. TITLE *(and Subtitle)* EFFECTS OF R-RATIO ON CRACK INITIATION AT EXTERNAL DISCONTINUITIES IN AUTOFRETTAGED CYLINDERS		5. TYPE OF REPORT & PERIOD COVERED Final
		6. PERFORMING ORG. REPORT NUMBER
7. AUTHOR(s) Robert R. Fujczak		8. CONTRACT OR GRANT NUMBER(s)
9. PERFORMING ORGANIZATION NAME AND ADDRESS US Army Armament Research & Development Command Benet Weapons Laboratory, DRDAR-LCB-TL Watervliet, NY 12189		10. PROGRAM ELEMENT, PROJECT, TASK AREA & WORK UNIT NUMBERS AMCMS No. 61110191A0011 DA Project No. 1L161101A9A PRON No. 1A2231491A1A
11. CONTROLLING OFFICE NAME AND ADDRESS US Army Armament Research & Development Command Large Caliber Weapon Systems Laboratory Dover, NJ 07801		12. REPORT DATE July 1982
		13. NUMBER OF PAGES 24
14. MONITORING AGENCY NAME & ADDRESS*(if different from Controlling Office)*		15. SECURITY CLASS. *(of this report)* UNCLASSIFIED
		15e. DECLASSIFICATION/DOWNGRADING SCHEDULE

16. DISTRIBUTION STATEMENT *(of this Report)*

Approved for public release; distribution unlimited.

17. DISTRIBUTION STATEMENT *(of the abstract entered in Block 20, if different from Report)*

19. KEY WORDS *(Continue on reverse side if necessary and identify by block number)*

Positive Stress Ratios	Stress Concentration
Autofrettage	Fatigue Strength Reduction Factor
Fatigue Crack Initiation	Modified Goodman Diagram
Residual Tensile Stresses	

20. ABSTRACT *(Continue on reverse side if necessary and identify by block number)*

Experimental work shows the effects of positive stress ratios, or tensile minimum stress, during the fatigue cycle on the fatigue crack initiation from holes. This simulates the effect of the residual tensile stresses at the outside surface of autofrettaged cylinders. S-N (stress life) curves and modified Goodman diagrams are shown for fatigue crack initiation.

DD FORM 1 JAN 73 **1473** EDITION OF 1 NOV 65 IS OBSOLETE

TABLE OF CONTENTS

LIST OF ILLUSTRATIONS

i

ACKNOLWEDGEMENTS

I wish to thank J. Throop for his technical guidance, R. Abbott for assistance in the testing program, and Ellen Fogarty for manuscript typing.

LIST OF SYMBOLS

a = inside radius of cylinder

(a) = approximate hole diameter in bend specimens

b = outside radius of cylinder

h = thickness of bend specimens

I = logarithmic value of Y-intercept from S-N curve

N_i = number of cycles for fatigue crack initiation

K_f = fatigue strength reduction factor

K_t = stress concentration factor

$K_{t\infty}$ = stress concentration factor for infinite width plate

p = internal pressure on cylinder

R = stress ratio between minimum stress and maximum stress

r = any radius between the inside and outside radius of cylinder

S = slope of S-N curve

W = cylindrical wall ratio between outside and inside diameter

σ_{alt} = alternating stress

$\overline{\sigma}_{alt}$ = alternating stress times the fatigue strength reduction factor K_f

σ_{max} = maximum stress

$\overline{\sigma}_{max}$ = maximum stress times the fatigue strength reduction factor K_f

σ_{mean} = mean stress

$\overline{\sigma}_{mean}$ = mean stress times the fatigue strength reduction factor K_f

σ_{min} = minimum stress

$\overline{\sigma}_{min}$ = minimum stress times the fatigue strength reduction factor K_f

σ_{tR} = tangential residual stress resulting from overstrain or autofrettage

σ_{tp} = tangential stress resulting from internal pressurization

σ_Y = yield strength of material

INTRODUCTION

The benefits of autofrettage on fatigue crack propagation of cracks have been well documented.[1] The reason behind these benefits is the compressive residual stress field on the inside wall of the cylinder after overpressurization has caused plastic deformation from the inside out. This allows a tremendous advantage in retarding crack initiation and propagation in the early stages of crack growth, accounting for the dramatic increases in useful service life for an autofrettaged cylinder compared to a non-autofrettaged cylinder.

However, because of the principles of equilibrium, the residual stresses on the outside surface are tensile in nature. This may be a cause of concern when external flaws such as holes, keyways, and notches are machined on the outside surface because of engineering design considerations, especially when an additional tensile stress is added on the outside surface from internal pressurization. Depending on the stress concentration effects and the fatigue strength reduction factor, this stress situation on the outside wall may take a heavy toll on the useful service life of the cylinder. In this study we will examine the effects of threaded holes on the outside surface.

R-RATIO

Figure 1 shows the relationship between the minimum stress and maximum stress, called the stress ratio, or the R-ratio.[2] In fully reversed loading

[1]Davidson, T. E., Kendall, D. P., and Reiner, A. N., "Residual Stresses in Thick-Walled Cylinders Resulting From Mechanically Induced Overstrain," Experimental Mechanics, November 1963.
[2]Richards, C. W., Engineering Materials Science, Wadsworth Publishing Company, Belmont, CA, 1967.

(Figure 1a), $R = -1$, as shown by the complete reversal of sign of the amplitude. Bending stresses in a rotating axle vary in this manner. Also, the mean stress is zero. When there is a combination of a constant load and an alternating load, the mean stress is no longer zero and the value of R may increase from -1 to zero (Figure 1b), where σ_{min} reaches zero. As R increases from zero to 1, σ_{min} becomes more tensile (Figure 1c). It is this last combination of loading that corresponds to the loading conditions on the outside of an autofrettaged cylinder caused by tensile residual stress and pressurization. This third case will be studied in this report.

APPARATUS AND PROCEDURE

The specimen configuration chosen to represent tensile stresses on the outside wall of a cylinder was a bending beam specimen one half inch (12.7 mm) thick by one inch (25.4 mm) wide, shown in Figure 2. Approximately 90 specimens were fabricated from sections of modified 4330 gun steel taken from a 155 mm cylinder. Representative material properties were: 0.1% offset yield strength = 160 Ksi (1100 MPa), ultimate tensile strength = 195 Ksi (1345 MPa), % elongation = 16%, % reduction in area = 50%.

One half of the specimens were fabricated with a 5/16 inch-24 UNF threaded hole and the second half were fabricated with a 6-32 UNC threaded hole. All holes were terminated at the middle, or neutral axis of the specimen. Stresses were calculated by using equations of bending beams in a combination of cross-sections approximating those of the test specimens.

All specimens were tested in a Sonntag SF1U fatigue testing machine with a nine inch (22.9 cm) lever arm bending fixture, or the five-to-one multiplier

fixture and a three inch (7.6 cm) lever arm. All specimens were fatigued until an arbitrary fatigue crack length of 0.050 inch (1.27 mm) on the tensile surface was detected and the number of cycles N_i was recorded. This was considered a reasonable upper limit on fatigue crack size for initiation because a crack of this size is still small but detectable by optical methods. In cases where no crack could be detected for greater than several million cycles, these specimens were considered runouts. The combination of static preload and dynamic alternating load allowed for an infinite variety of values for R-ratio, but in our case only positive values were used to evaluate the stress conditions seen on the outside surface of autofrettaged cylinders subject to internal pressurization.

Figure 3 shows some ranges of stresses on the outer surface of typical cylinders for the 100 percent overstrained condition. This shows residual tensile from about 70 Ksi (483 MPa) to about 105 Ksi (724 MPa) and stress ranges caused by pressure from about 28 Ksi (193 MPa) to about 60 Ksi (414 MPa). The stress figures in parentheses in Figure 3 are the values of internal pressure.

STRESS EQUATIONS

In order to calculate the final value of stress caused by combination of external residual tensile stress and Lame' circumferential stress caused by internal pressurization, the following equations were used.
External residual tensile stress for 100 percent overstrain condition:[2]

---

[2]Richards, C. W., Engineering Materials Science, Wadsworth Publishing Company, Inc., Belmont, CA, 1967.

3

$$\frac{\sigma_{tR}}{\sigma_Y} = \frac{-\ell nW}{W^2-1} (1 + \frac{b^2}{r^2}) + (1 - \ell n \frac{b}{r}) \qquad (1)$$

At r = b:

$$\frac{\sigma_{tR}}{\sigma_Y} = \frac{-2\ell nW}{W^2-1} + 1 \qquad (2)$$

Pressure stress:

$$\sigma_{tp} = \frac{a^2p}{(b^2-a^2)} (1 + \frac{b^2}{r^2}) \qquad (3)$$

At r = b:

$$\sigma_{tp} = \frac{2p}{(W^2-1)} \qquad (4)$$

The combination of Eqs. (2) and (4) provides the maximum stress on the outside surface of the 100 percent overstrained cylinder.

TEST SCHEDULE

Figure 4 shows the relationship between minimum stress, mean stress and alternating stress for all ranges of positive R-ratio considered. Also shown are the locations on this plot for the cylinders shown in Figure 3. The residual tensile stress on the outside of the cylinder is represented by σ_{min} in Figure 4. The Lame' stress caused by pressurization is represented by σ_{alt}. Thus, for any particular stress ratio, the appropriate values of σ_{min}, σ_{alt}, and σ_{mean} may be calculated by referring to the graph parameters.

The test schedule was designed using Figure 4 at varying stress ratio levels with stress conditions as severe as the examples shown from Figure 3 or more severe conditions in order to obtain a wide range of fatigue crack

initiation cycles. Figure 5 shows the test matrix used. The arrows labelled N_i show the direction in which N_i will be increased.

STRESS CONCENTRATION FACTORS

The following stress concentration factors for simple bending of an infinite width plate[3] with a hole were used to determine K_t for holes in bending of finite width plates.

For $(a)/h \rightarrow \infty$:

$$K_{t\infty} = \frac{5+3\nu}{3+\nu} \qquad (5)$$

For $\nu = 0.3$ (steel), $K_{t\infty} = 1.788$.

For the large threaded hole (5/16 inch-24 UNF), the approximate value for the hole size (a) used was 0.3 inch (7.62 mm). So for $(a)/h = 0.6$, the value of $K_{t\infty}$ was:

$$K_{t\infty} = 2.45 \text{ (large hole)}$$

For the small threaded hole (6-32 UNC), an approximate value of (a) = 0.1278 inch (3.246 mm) was used. So for $(a)/h = 0.2556$, the value of K_t was:

$$K_{t\infty} = 2.72 \text{ (small hole)}$$

Using these values of $K_{t\infty}$ and (a)/h the following values of K_t for finite width plate were found from Peterson:[3]

$$K_t = 1.9 \text{ (large hole)}$$

$$K_t = 2.4 \text{ (small hole)}$$

---

[3]Peterson, R. E., Stress Concentration Factors, John Wiley and Sons, New York, 1974.

It can be seen that the stress concentration factor for the small hole is greater than that for the large hole, signifying a more serious stress concentration as the hole diameter decreases. However, the worst case deteriorates only to $K_t = 3$ for a hole in transverse bending of a plate.[3]

FATIGUE NOTCH FACTOR

Lipson and Sheth[4] have shown a relationship between fatigue notch factor and stress concentration factor for steel and cast iron. From this relationship the following values for the two hole sizes were calculated:

$$K_f = 1.85 \text{ (large hole)}$$

$$K_f = 2.27 \text{ (small hole)}$$

RESULTS AND DISCUSSION

Figures 6 and 7 show the S-N (stress life) curves of alternating stress versus number of cycles to crack initiation and the least-squares data fits based on the stress concentration factors and fatigue notch factors derived above. Both conditions exhibit an apparent endurance limit at stress levels below 20 Ksi (138 MPa). Note that the large hole specimens allow fatigue crack initiation to occur at more than twice the cycles for fatigue crack initiation at the many holes under equivalent alternating stress levels.

Figures 6 and 7 exhibit a spread in the fatigue crack initiation data as shown by the funnel lines. Further analysis showed that this fanning out effect can be explained by the changes in stress ratio.

---

[3]Peterson, R. E., Stress Concentration Factors, John Wiley and Sons, New York, 1974.
[4]Lipson, C. and Sheth, N. J., Statistical Design and Analysis of Engineering Experiments, McGraw-Hill Book Company, NY, 1973.

6

To more fully describe the effects of stress ratio on fatigue crack initiation, Figure 8 shows the changes in slope and Y-intercept of the lines on log-log graph of the S-N curve in Figures 6 and 7 caused by changes in stress ratio. The lines have a slope, S, which represents the power term of $\bar{\sigma}_{alt}$, and a Y-intercept, I, which represents the coefficient of $\bar{\sigma}_{alt}$, and may be expressed as follows:

$$\ln N_i = S \ln \bar{\sigma}_{alt} + I \qquad (6)$$

As seen in Figure 8, the slope increases from -4.72 at R = 0 to -3.15 at R = 0.7, and the value of I decreases from 31.7 at R = 0 to 24.3 at R = 0.7.

Figure 9 shows the effects of stress ratio R on fatigue crack initiation. $\bar{\sigma}_{alt}$ is the alternating stress value with K_f taken into consideration. By multiplying the nominal alternating stress by K_f, one may obtain an average value of fatigue crack initiation life from this graph. Please note that for lives greater than 12,000 fatigue cycles the graph shows that as the stress ratio increases while σ_{alt} is kept constant, the number of cycles to initiate the fatigue crack decreases, indicating the suppressive effect of increasing the R-ratio. Since the data converges at about 12,000 cycles, this shows that the R-ratio has significantly less effect on crack initiation than the change in alternating stress in this intermediate cycle range. The R-ratio effect becomes more dominant in the high cycle range. Insufficient data was generated in the low cycle range to determine which has the dominant effect, but it appears to be the alternating stress from the trend of the limited data available.

By using an interactive set of stress coordinates, one can describe the fatigue crack initiation in terms of any two stress parameters by aligning the stress and scaling them as shown in Figure 10. This diagram was developed in Reference 5.

Solving Eq. (6) for $\bar{\sigma}_{alt}$ by using a root finder technique, one can plot the modified Goodman diagram shown in Figure 10 with constant fatigue initiation cycle parameters. This diagram can then be used to determine average fatigue initiation life for any stress conditions for positive stress ratios, taking into account the fatigue strength reduction factor for the external holes studied. The designer may use the diagram to predict the average useful fatigue life of a component with a threaded hole subject to positive stress ratios if the value of K_f is known for the hole size.

CONCLUSIONS

1. The effect of hole size in fatigue crack initiation is directly related to the fatigue notch factor. The smaller the hole diameter, the lower the number of cycles required to initiate a fatigue crack at the hole.

2. For positive values of stress ratio, an increase in the R-ratio decreases the number of cycles to initiate a fatigue crack while the alternating stress is kept constant.

3. By taking into account the fatigue notch factor, one may predict the average initiation life for a range of hole sizes under positive stress ratio conditions by using a single modified Goodman diagram with the appropriate curves for the material used.

----

[5]Burk, J. D. and Lawrence, F. V., "The Effect of Residual Stresses on Weld Fatigue Life," Fracture Control Program Report No. 29, College of Engineering, University of Illinois, Urbana, IL, January 1978.
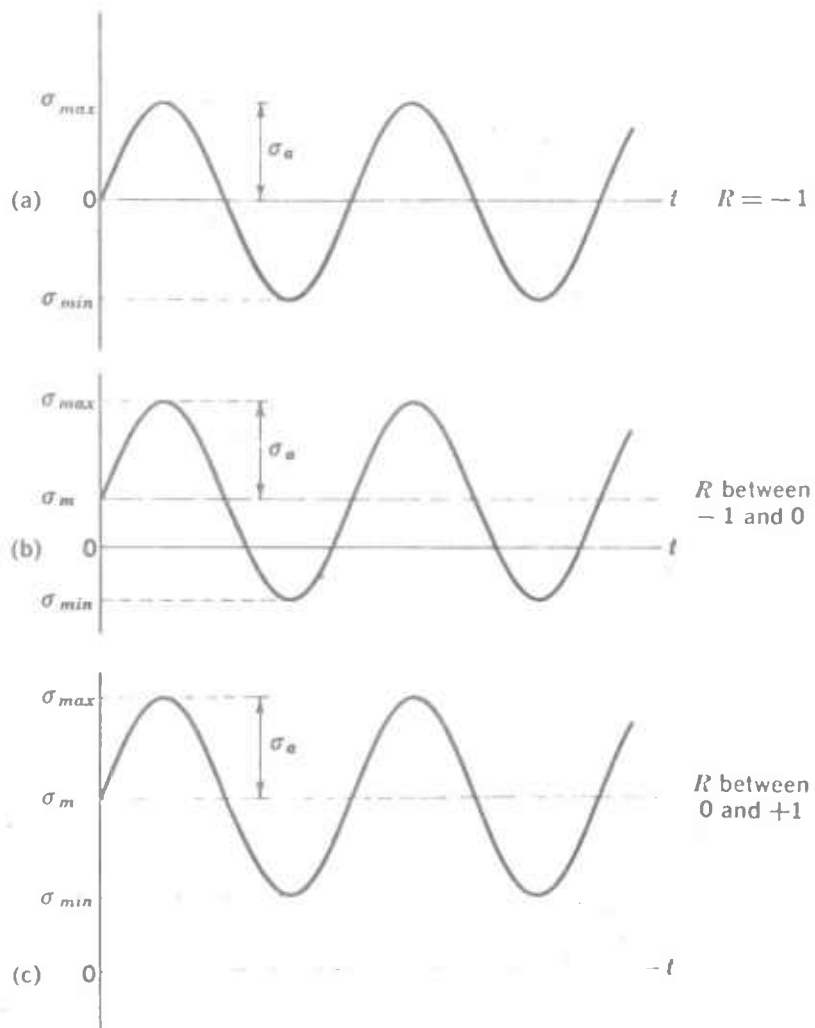
REFERENCES

1. Davidson, T. E., Kendall, D. P., and Reiner, A. N., "Residual Stresses in Thick-Walled Cylinders Resulting From Mechanically Induced Overstrain," Experimental Mechanics, November 1963.

2. Richards, C. W., Engineering Materials Science, Wadsworth Publishing Company, Inc., Belmont, CA, 1967.

3. Peterson, R. E., Stress Concentration Factors, John Wiley and Sons, New York, 1974.

4. Lipson, C. and Sheth, N. J., Statistical Design and Analysis of Engineering Experiments, McGraw-Hill Book Company, NY, 1973.

5. Burk, J. D. and Lawrence, F. V., "The Effect of Residual Stresses on Weld Fatigue Life," Fracture Control Program Report No. 29, College of Engineering, University of Illinois, Urbana, IL, January 1978.

Figure 1.   General Relationships Between Minimum and Maximum Stress.
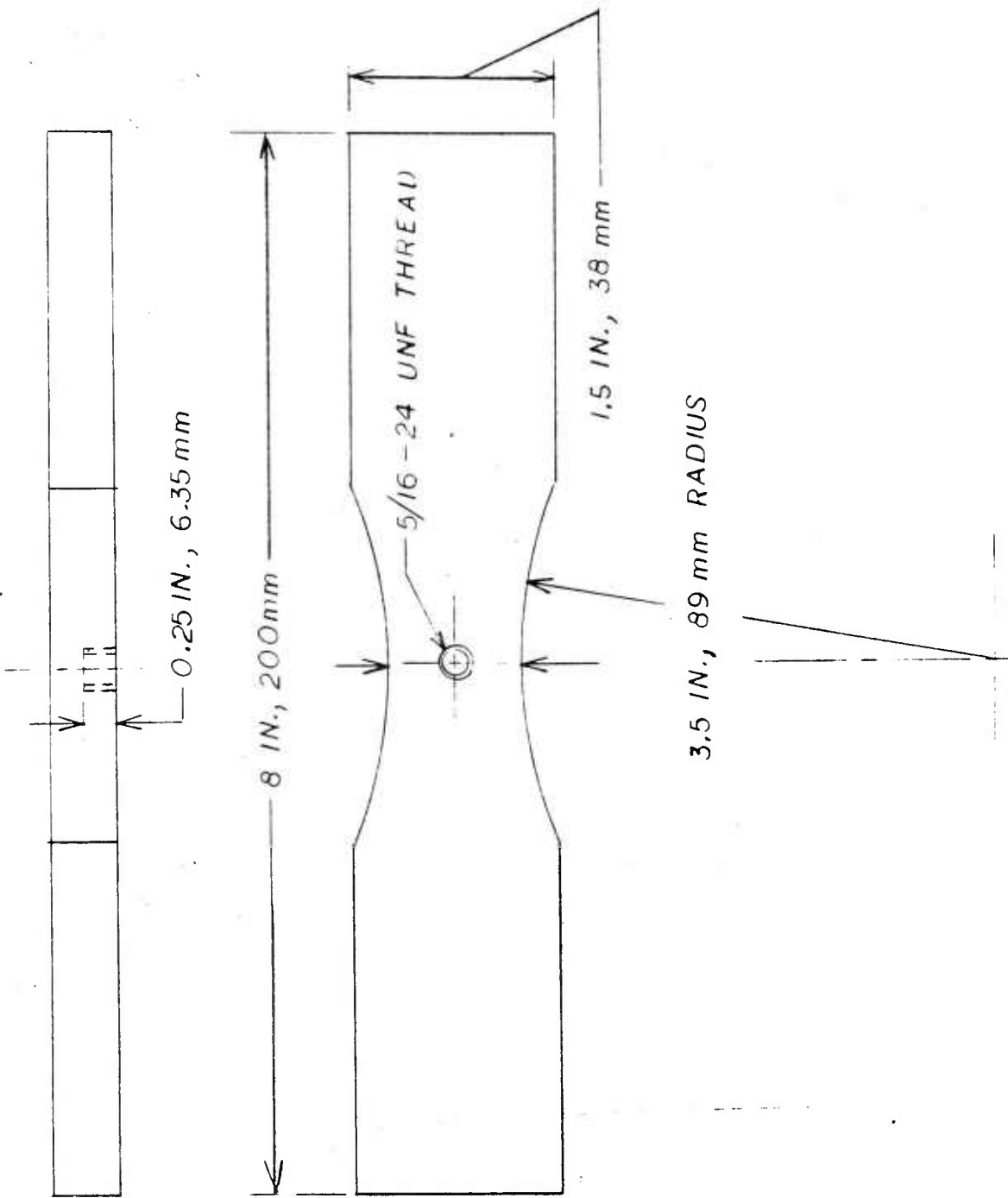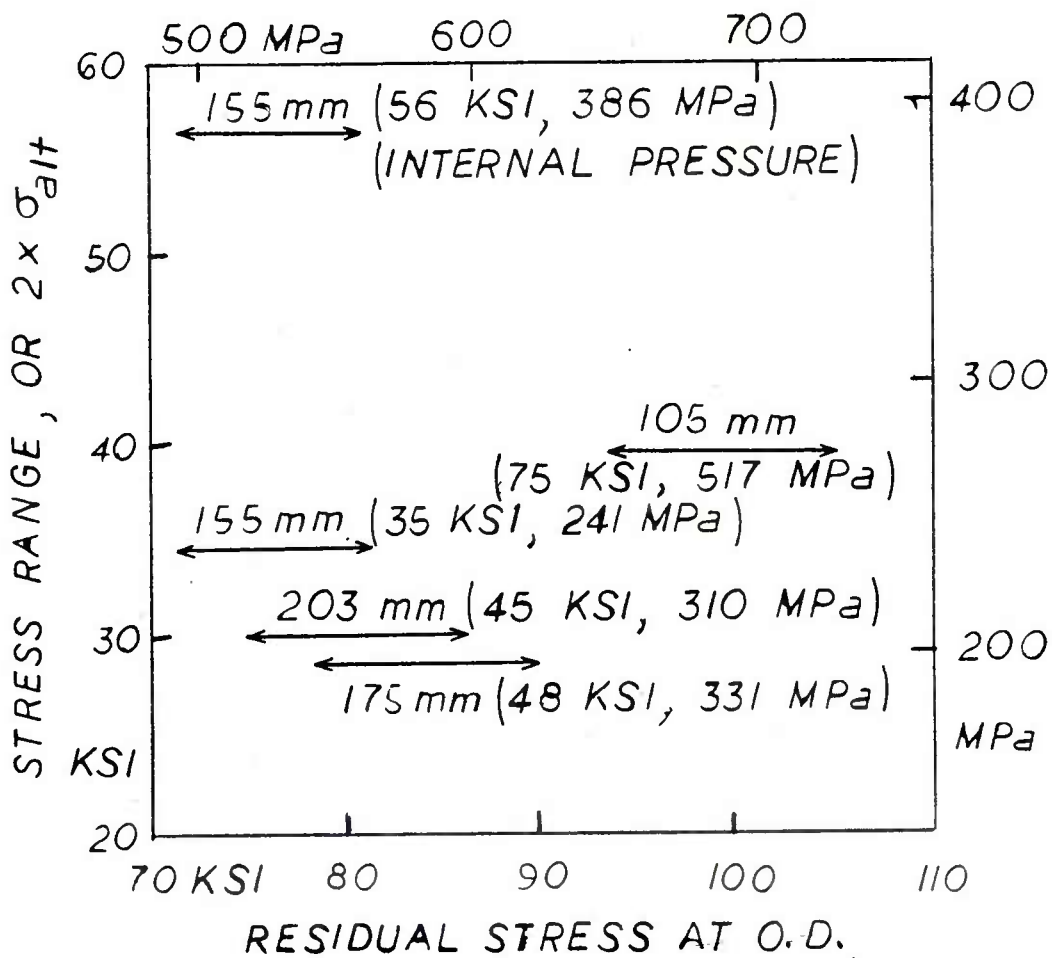
0.25 IN., 6.35 mm

8 IN., 200mm

5/16 - 24 UNF THREAD

1.5 IN., 38 mm

3.5 IN., 89 mm RADIUS

Figure 2. Bending Specimen Configuration with Large Hole.

11

Figure 3. Range of Stresses on the Outer Surface of Typical Cylinders.
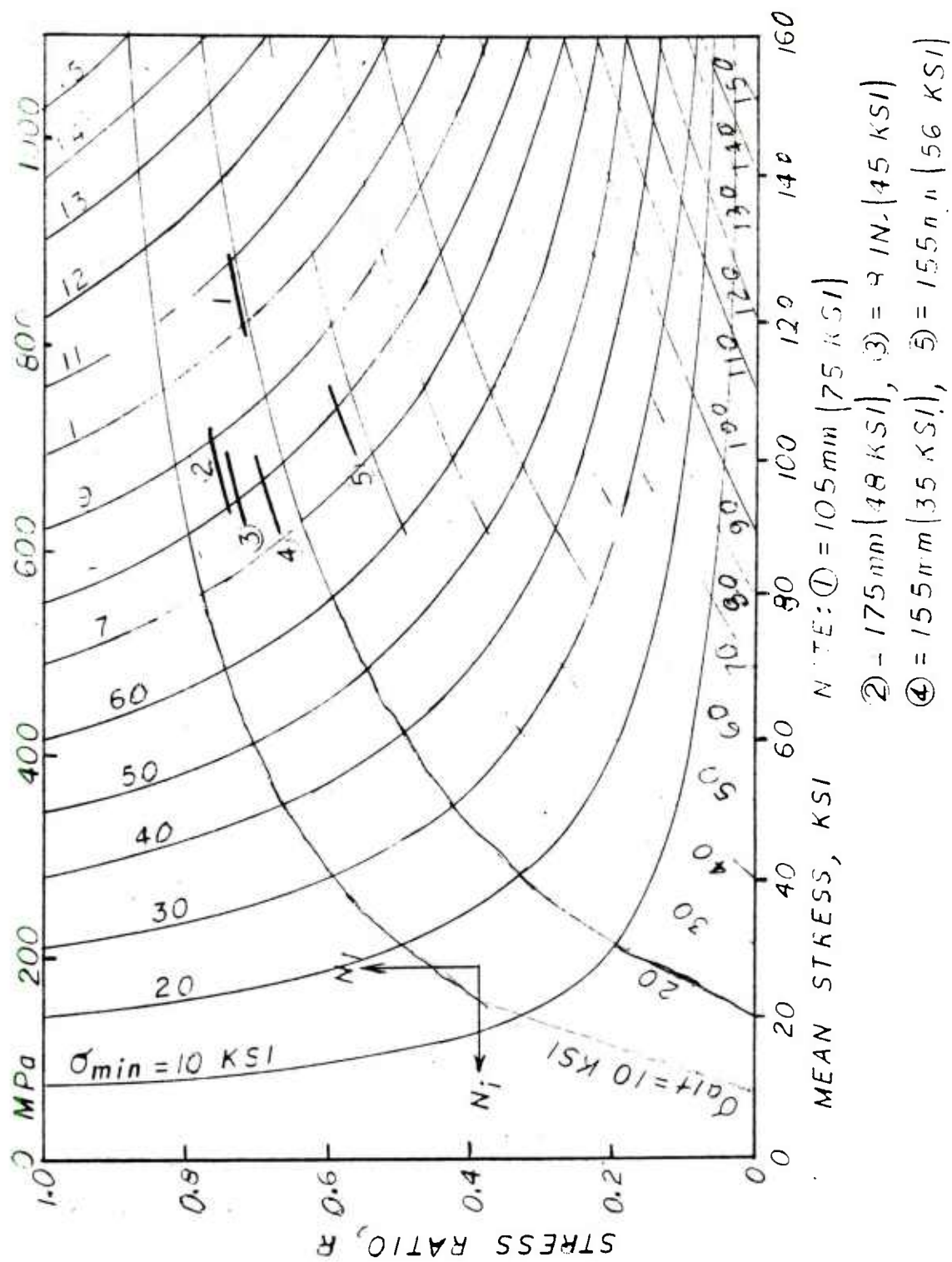
Figure 4. Relationship Between Minimum Stress, Mean Stress, and Alternating Stress for Positive Stress Ratios.
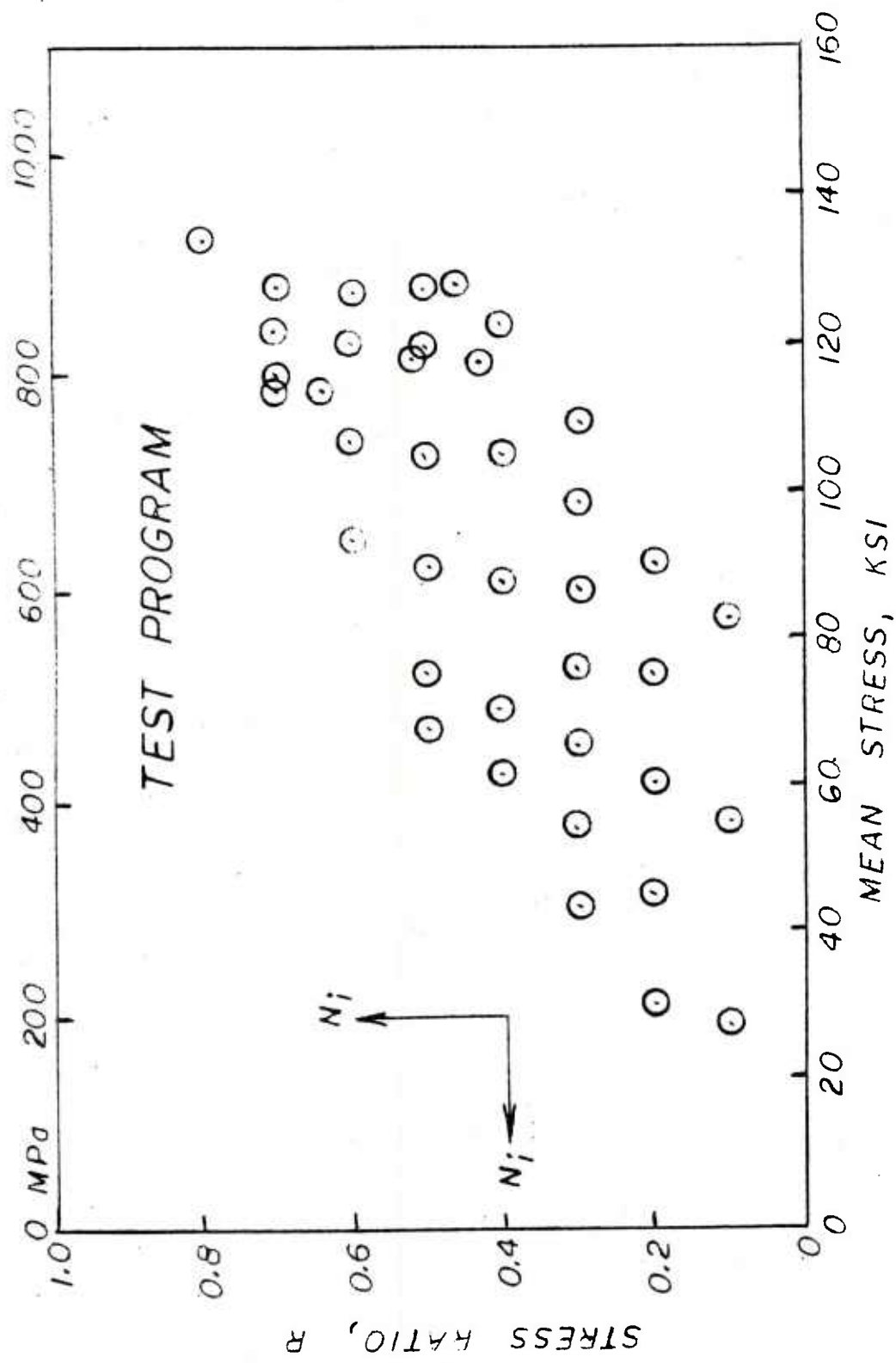
13

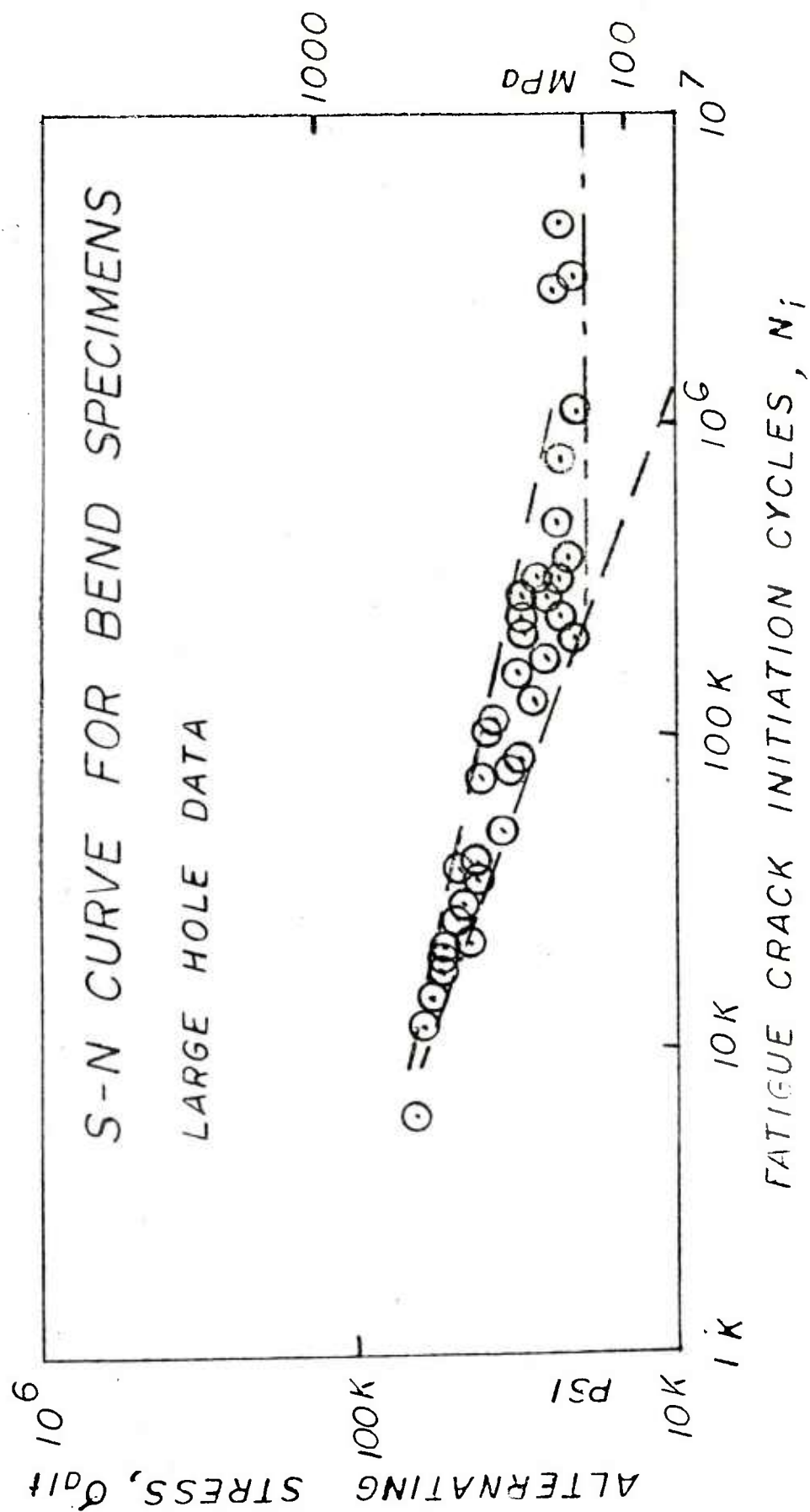Figure 5. Test Data Matrix for Each Stress Ratio.

Figure 6.   S-N Curve for Large Hole Bend Specimens.

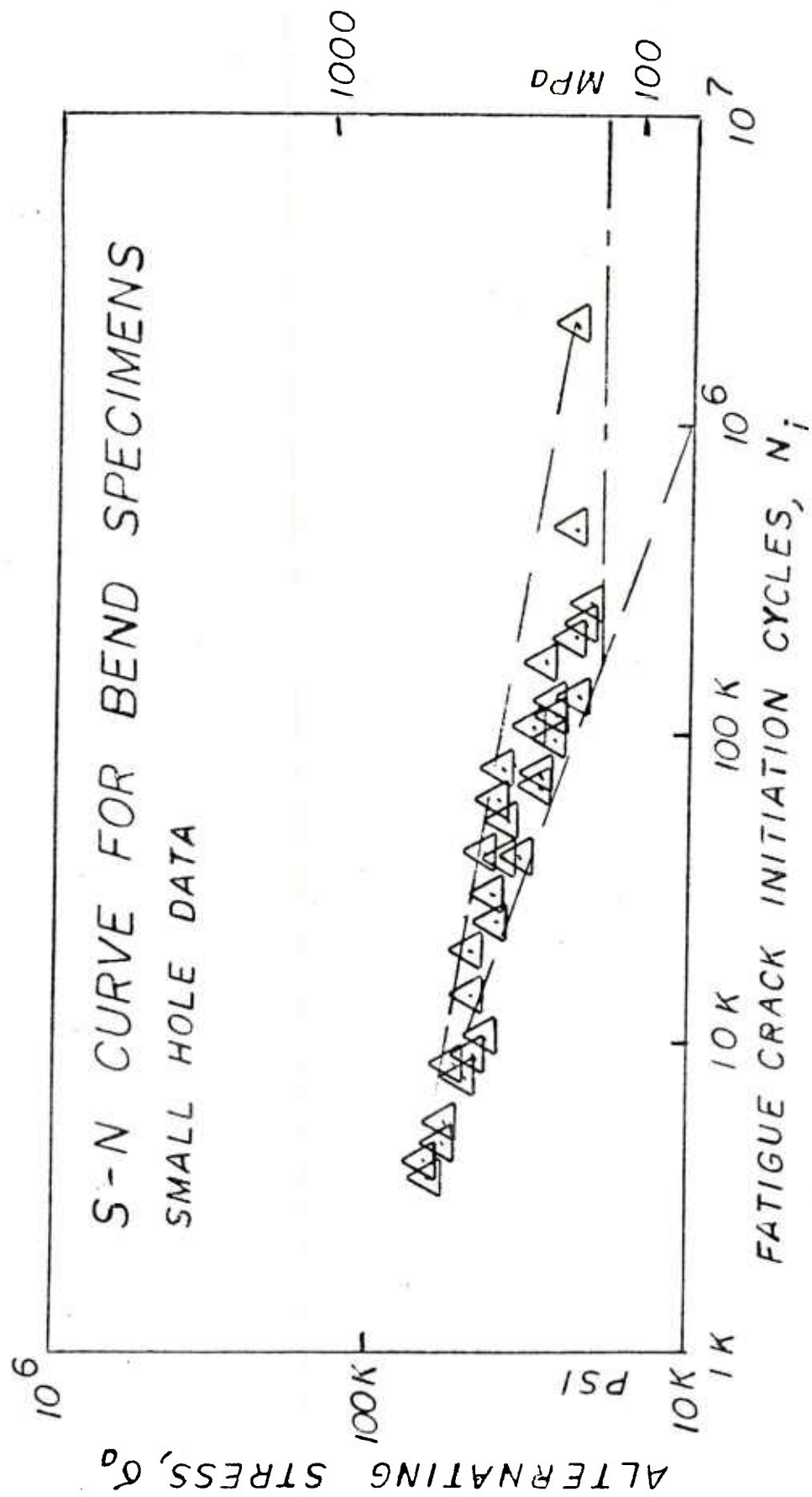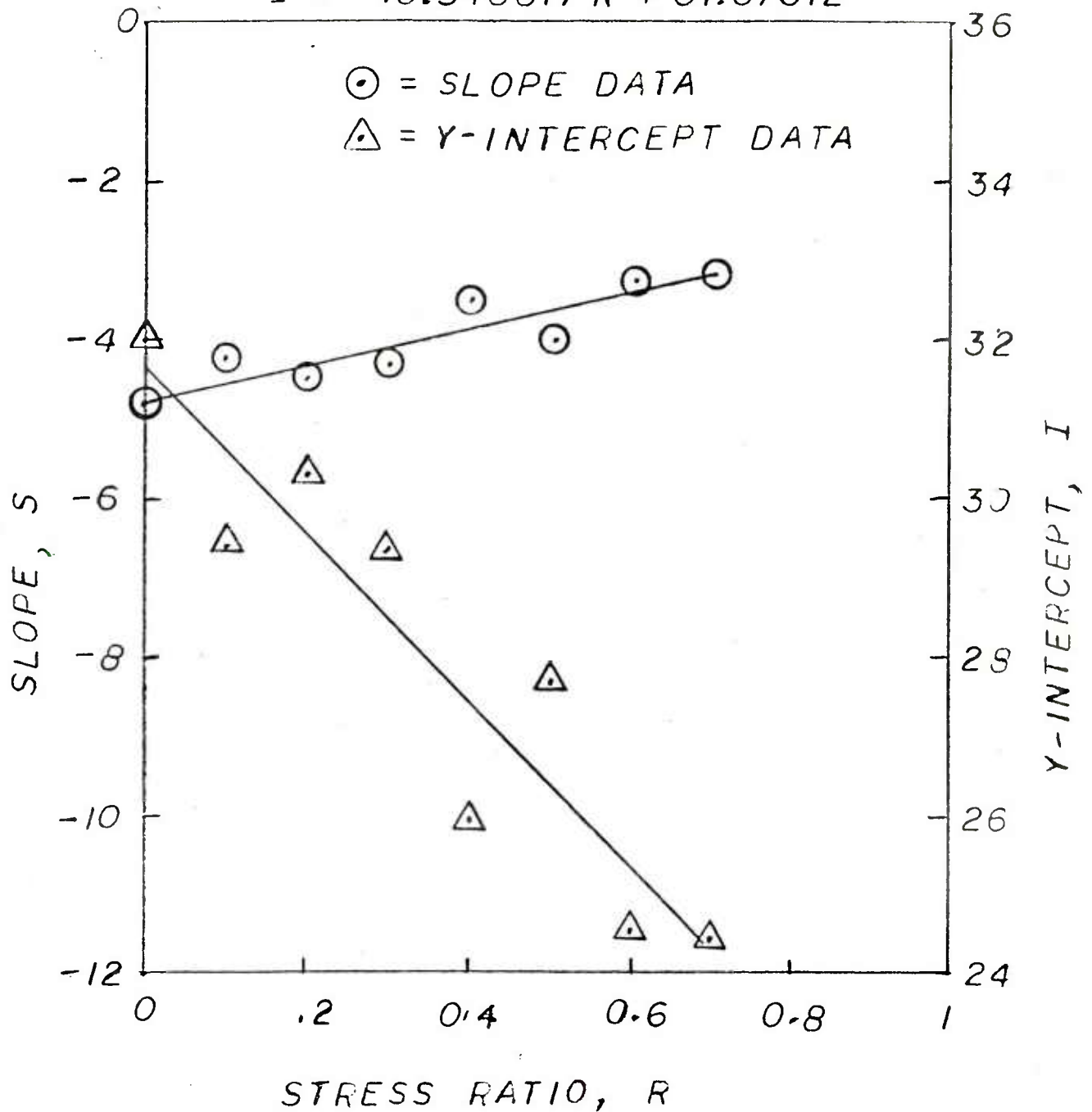Figure 7.   S-N Curve for Small Hole Bend Specimens.

Figure 8. Variation of Slope and Y-Intercept from S-N Curves Caused by Change in Stress Ratio.
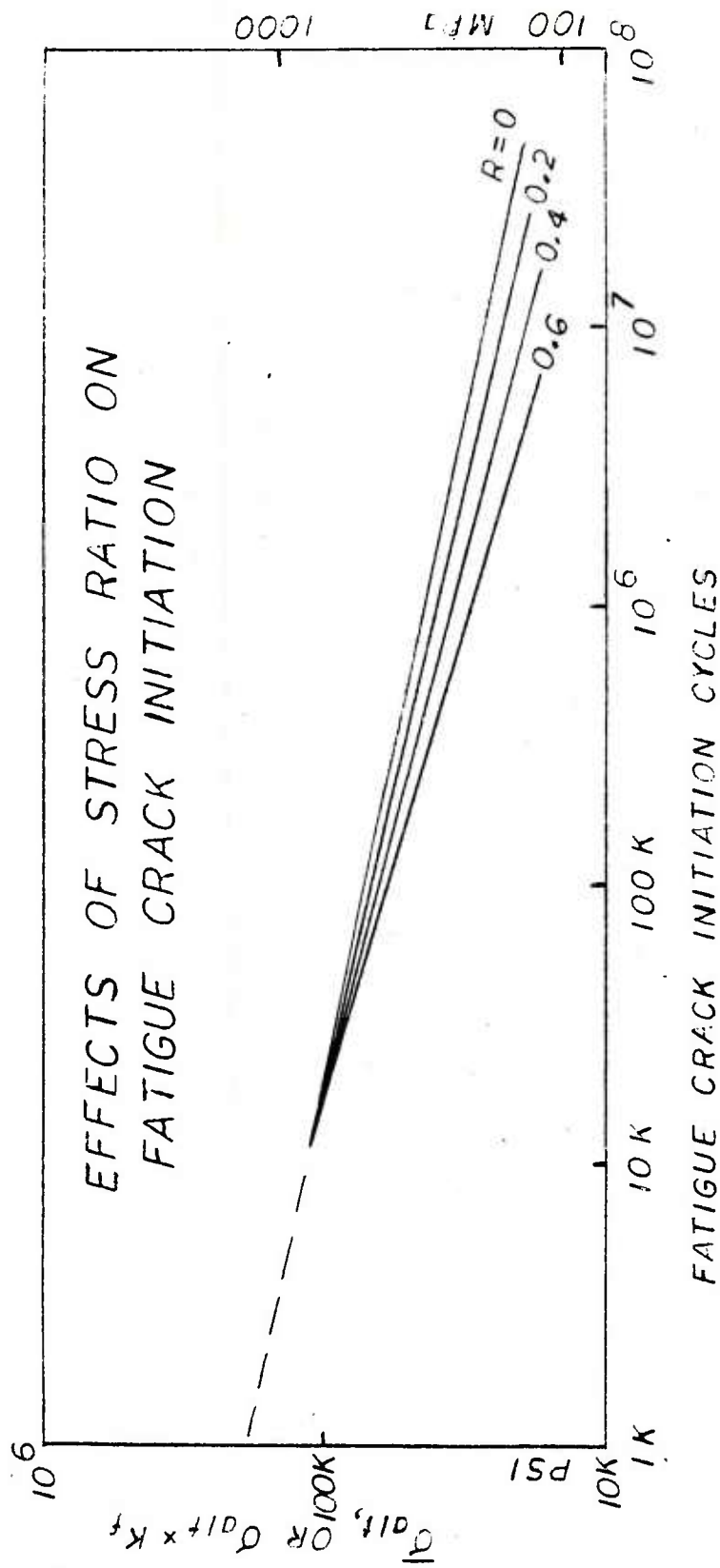
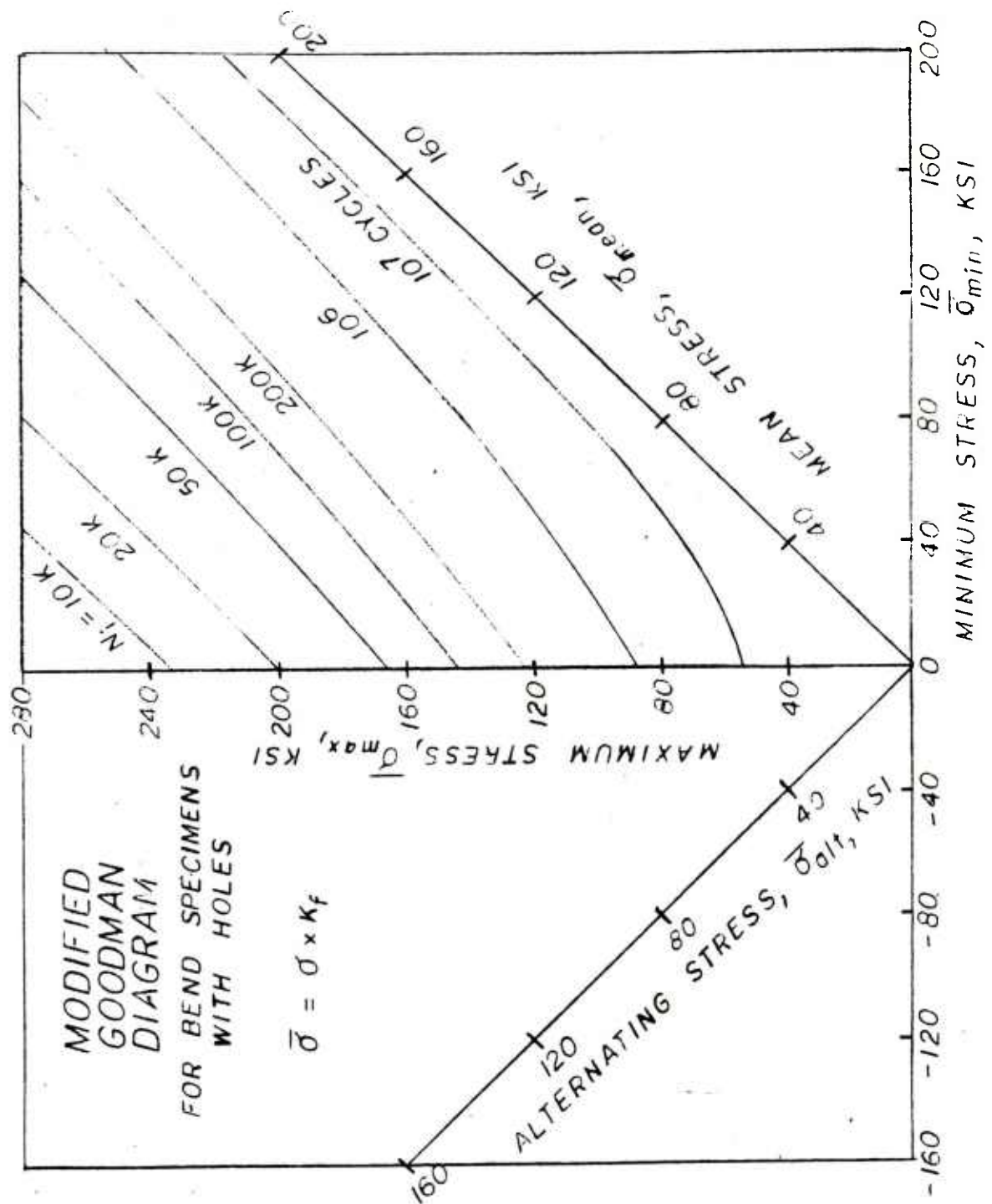Figure 9. Effects of Stress Ratio on Fatigue Crack Initiation on S-N Curve Incorporating K_f.

18

Figure 10. Modified Goodman Diagram for Bend Specimens with Holes Incorporating K_f.

TECHNICAL REPORT INTERNAL DISTRIBUTION LIST

	NO. OF COPIES
COMMANDER	1
CHIEF, DEVELOPMENT ENGINEERING BRANCH	1
ATTN: DRDAR-LCB-DA	1
-DM	1
-DP	1
-DR	1
-DS (SYSTEMS)	1
-DS (ICAS GROUP)	1
-DC	1
CHIEF, ENGINEERING SUPPORT BRANCH	1
ATTN: DRDAR-LCB-SE	1
-SA	1
CHIEF, RESEARCH BRANCH	2
ATTN: DRDAR-LCB-RA	1
-RC	1
-RM	1
-RP	1
TECHNICAL LIBRARY	5
ATTN: DRDAR-LCB-TL	
TECHNICAL PUBLICATIONS & EDITING UNIT	2
ATTN: DRDAR-LCB-TL	
DIRECTOR, OPERATIONS DIRECTORATE	1
DIRECTOR, PROCUREMENT DIRECTORATE	1
DIRECTOR, PRODUCT ASSURANCE DIRECTORATE	1

NOTE: PLEASE NOTIFY DIRECTOR, BENET WEAPONS LABORATORY, ATTN: DRDAR-LCB-TL, OF ANY REQUIRED CHANGES.

TECHNICAL REPORT EXTERNAL DISTRIBUTION LIST

	NO. OF COPIES		NO. OF COPIES
ASST SEC OF THE ARMY RESEARCH & DEVELOPMENT ATTN: DEP FOR SCI & TECH THE PENTAGON WASHINGTON, D.C. 20315	1	COMMANDER US ARMY TANK-AUTMV R&D COMD ATTN: TECH LIB - DRDTA-UL MAT LAB - DRDTA-RK WARREN, MICHIGAN 48090	1 1
COMMANDER US ARMY MAT DEV & READ. COMD ATTN: DRCDE 5001 EISENHOWER AVE ALEXANDRIA, VA 22333	1	COMMANDER US MILITARY ACADEMY ATTN: CHMN, MECH ENGR DEPT WEST POINT, NY 10996	1

COMMANDER
US ARMY ARRADCOM
ATTN: DRDAR-LC
        -LCA (PLASTICS TECH
            EVAL CEN)
        -LCE
        -LCM
        -LCS
        -LCW
        -TSS (STINFO)
DOVER, NJ 07801
	1
	1
	1
	1
	1
	1
	2
		US ARMY MISSILE COMD
		REDSTONE SCIENTIFIC INFO CEN
		ATTN: DOCUMENTS SECT, BLDG 4484
		REDSTONE ARSENAL, AL 35898
			2

		COMMANDER REDSTONE ARSENAL ATTN: DRSMI-RRS -RSM ALABAMA 35809	1 1
COMMANDER US ARMY ARRCOM ATTN: DRSAR-LEP-L ROCK ISLAND ARSENAL ROCK ISLAND, IL 61299	1	COMMANDER ROCK ISLAND ARSENAL ATTN: SARRI-ENM (MAT SCI DIV) ROCK ISLAND, IL 61299	1
DIRECTOR US ARMY BALLISTIC RESEARCH LABORATORY ATTN: DRDAR-TSB-S (STINFO) ABERDEEN PROVING GROUND, MD 21005	1	COMMANDER HQ, US ARMY AVN SCH ATTN: OFC OF THE LIBRARIAN FT RUCKER, ALABAMA 36362	1
COMMANDER US ARMY ELECTRONICS COMD ATTN: TECH LIB FT MONMOUTH, NJ 07703	1	COMMANDER US ARMY FGN SCIENCE & TECH CEN ATTN: DRXST-SD 220 7TH STREET, N.E. CHARLOTTESVILLE, VA 22901	1
COMMANDER US ARMY MOBILITY EQUIP R&D COMD ATTN: TECH LIB FT BELVOIR, VA 22060	1	COMMANDER US ARMY MATERIALS & MECHANICS RESEARCH CENTER ATTN: TECH LIB - DRXMR-PL WATERTOWN, MASS 02172	2

NOTE: PLEASE NOTIFY COMMANDER, ARRADCOM, ATTN: BENET WEAPONS LABORATORY,
      DRDAR-LCB-TL, WATERVLIET ARSENAL, WATERVLIET, N.Y. 12189, OF ANY
      REQUIRED CHANGES.

	NO. OF COPIES		NO. OF COPIES
COMMANDER US ARMY RESEARCH OFFICE P.O. BOX 12211 RESEARCH TRIANGLE PARK, NC 27709	1	COMMANDER DEFENSE TECHNICAL INFO CENTER ATTN: DTIA-TCA CAMERON STATION ALEXANDRIA, VA 22314	12 (2-LTD)
COMMANDER US ARMY HARRY DIAMOND LAB ATTN: TECH LIB 2800 POWDER MILL ROAD ADELPHIA, MD 20783	1	METALS & CERAMICS INFO CEN BATTELLE COLUMBUS LAB 505 KING AVE COLUMBUS, OHIO 43201	1
DIRECTOR US ARMY INDUSTRIAL BASE ENG ACT ATTN: DRXPE-MT ROCK ISLAND, IL 61299	1	MECHANICAL PROPERTIES DATA CTR BATTELLE COLUMBUS LAB 505 KING AVE COLUMBUS, OHIO 43201	1
CHIEF, MATERIALS BRANCH US ARMY R&S GROUP, EUR BOX 65, FPO N.Y. 09510	1	MATERIEL SYSTEMS ANALYSIS ACTV ATTN: DRXSY-MP ABERDEEN PROVING GROUND MARYLAND 21005	1
COMMANDER NAVAL SURFACE WEAPONS CEN ATTN: CHIEF, MAT SCIENCE DIV DAHLGREN, VA 22448	1		
DIRECTOR US NAVAL RESEARCH LAB ATTN: DIR, MECH DIV CODE 26-27 (DOC LIB) WASHINGTON, D.C. 20375	1 1		
NASA SCIENTIFIC & TECH INFO FAC P.O. BOX 8757, ATTN: ACQ BR BALTIMORE/WASHINGTON INTL AIRPORT MARYLAND 21240	1		

NOTE: PLEASE NOTIFY COMMANDER, ARRADCOM, ATTN: BENET WEAPONS LABORATORY,
DRDAR-LCB-TL, WATERVLIET ARSENAL, WATERVLIET, N.Y. 12189, OF ANY
REQUIRED CHANGES.